COMMUNICATION

Check for updates

One-step plasma-enabled catalytic carbon dioxide hydrogenation to higher hydrocarbons: significance of catalyst-bed configuration†

Jiajie Wang,[a,b] Mohammad S. AlQahtani, [a,c] Xiaoxing Wang, *[a]
Sean D. Knecht, [d] Sven G. Bilén, [d,e] Chunshan Song *[a,c,f] and Wei Chu [b]

Effectively converting CO_2 into fuels and value-added chemicals remains a major challenge in catalysis, especially under mild conditions. In this study, we report a one-step plasma-enabled catalytic process for CO_2 hydrogenation to C_2^+ hydrocarbons operated at low temperature and atmospheric pressure in a dielectric barrier discharge (DBD) packed-bed reactor. Plasma without catalyst produces mainly CO (over 80% selectivity), while CH_4 becomes the main product when plasma is coupled with the alumina-supported Co catalyst. Interestingly, by simply changing the catalyst-bed configuration within the plasma discharge zone, more C_2^+ hydrocarbons are selectively produced. High C_2^+ hydrocarbons selectivity of 46% at *ca.* 74% CO_2 conversion is achieved when operated at the furnace temperature of 25 °C and 10 W DBD plasma. The possible origin of C_2^+ formation and the significance of catalyst-bed configuration are discussed.

Transforming waste CO_2 into chemicals and fuels offers not only a possible solution to mitigate anthropogenic CO_2 emissions, but also an alternative to alleviate dependence on fossil fuels,[1] supporting sustainable development and green chemistry.[1–6] CO_2 is thermodynamically stable ($\Delta G° = -393.5$ kJ mol^{-1}), thus preferably converted with a co-reactant having higher free Gibbs energy such as CH_4 ($\Delta G° = -50.7$ kJ mol^{-1}) and H_2 ($\Delta G° = 0$ kJ mol^{-1}).[1] CO_2 reaction with H_2 is thermodynamically favorable;[7] furthermore, H_2 can be pro-

duced from H_2O using renewable energy, which makes the overall process environmentally friendly.[1]

Much effort has been devoted to improving the performance of catalysts for producing higher hydrocarbons from CO_2.[8–11] C_2^+ hydrocarbons can be used as a liquid fuel or an entry platform (*e.g.*, light olefins) for existing chemical production chains.[12,13] In order to achieve high C_2^+ yield, high pressure (1.0–4.0 MPa) under the temperature of 200–400 °C is normally required.[2] Another critical issue in thermal-catalytic processes is the catalyst deactivation caused by metal sintering and carbon deposition.[14] Thus, achieving CO_2 activation and carbon chain growth under mild conditions remains a great challenge.[2,13]

Non-thermal plasma (NTP) provides a unique medium for performing catalytic CO_2 conversion at low temperatures owing to its non-equilibrium characteristics. Highly energetic electrons (1–10 eV) generated in NTP collide with gas molecules to produce highly reactive species (*i.e.*, ions, radicals, excited atoms and excited molecules), enabling thermodynamically and/or kinetically unfavored reactions at low temperatures.[15–17]

Although various catalysts, such as nickel,[18–20] cobalt,[21] copper,[7,22] platinum,[7] transition metal oxide[23] and molecular sieves,[21] have been studied for plasma-catalytic CO_2 hydrogenation during the past few decades,[1,16,24] CO and CH_4 are always the major products while the amount of C_2^+ is scarce. Only Lan *et al.* have achieved 13.7% selectivity of higher hydrocarbons over a Co/ZSM-5 catalyst.[21] Hence, the selective production of long-chain hydrocarbons from CO_2 hydrogenation using plasma-catalysis is still challenging.

Herein, we report a non-thermal plasma-driven catalytic process for one-step conversion of CO_2 and H_2 into higher hydrocarbons operated at low temperature and atmospheric pressure. We demonstrate the significance of catalyst-bed configuration within a dielectric barrier discharge (DBD) plasma discharge zone for the production of C_2^+ hydrocarbons on a γ-Al_2O_3 supported Co catalyst (the content of cobalt metal was fixed at 15 wt% based on the support, and termed as 15Co). To the best of our knowledge, it is the first report of plasma-enabled one-step CO_2 hydrogenation into C_2^+ hydrocarbons with C_2^+ selectivity over 46% at *ca.* 74% CO_2 conversion.

a Clean Fuels & Catalysis Program, EMS Energy Institute, Department of Energy and Mineral Engineering, The Pennsylvania State University, University Park, PA, 16802, USA. E-mail: xuw4@psu.edu, cxs23@psu.edu, chunshansong@cuhk.edu.hk
b Department of Chemical Engineering, Sichuan University, Sichuan, P.R. China
c Department of Chemical Engineering, The Pennsylvania State University, University Park, PA, 16802, USA
d School of Engineering Design, Technology, and Professional Programs, The Pennsylvania State University, University Park, PA, 16802, USA
e School of Electrical Engineering and Computer Science, The Pennsylvania State University, University Park, PA, 16802, USA
f Department of Chemistry, Faculty of Science, The Chinese University of Hong Kong, Shatin, Hong Kong, China
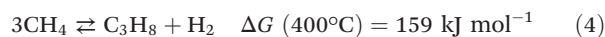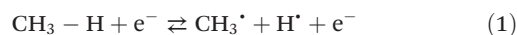†Electronic supplementary information (ESI) available. See DOI: 10.1039/d0gc03779f

Fig. 1a shows the CO_2 conversion and product selectivity in CO_2 hydrogenation under different operation modes including catalyst alone, plasma alone, and plasma-catalyst operated at the furnace temperature of 25 °C (no external heating). As expected, both 15Co catalyst and alumina support are thermally inactive at room temperature. Plasma alone initiates CO_2 hydrogenation at mild conditions with CO as the main product (over 80% selectivity), consistent with early reports.[7,23] Packing alumina in the discharge zone does not seem to affect the plasma performance. Coupling 15Co catalyst with plasma significantly changes the product distribution, as the methane selectivity increases significantly from 3% to 45%, while CO selectivity drops down to 38%. Additionally, a small amount of C_2^+ hydrocarbons (*ca.* 3% selectivity) is produced. Part of the observed changes could be attributed to plasma-induced thermal effects as the temperature inside the catalyst bed increased to 200 °C (Table S3†).

Although C_2^+ hydrocarbons are successfully obtained when operated at the furnace temperature of 25 °C (Fig. 1a), its selectivity is low. In order to get a more distinct result in C_2^+ production for accurate comparison, we have further operated the reactions at the furnace temperature of 250 °C. Fig. 1b illustrates the influence of increasing the furnace temperature to 250 °C, which reveals the possibility of obtaining more C_2^+

hydrocarbons. Under thermal reaction conditions, about 45% of CO_2 is converted over the 15Co catalyst, and methane is the main product (83% selectivity) along with traces of C_2^+ hydrocarbons (<1%). For an empty or alumina-packed reactor under plasma, both CO_2 conversion and CO selectivity do not show appreciable changes after raising the operating temperature to 250 °C. In contrast, a significant increase in CO_2 conversion (63%) and methane selectivity (81%) is observed over the 15Co catalyst under plasma. More importantly, the selectivity to C_2^+ hydrocarbons increases from 3% to 7%.

It should be pointed out that plasma can generate heat and thus cause the reactor temperature to rise. At the furnace temperature of 250 °C, unlike the thermal reactions where the reactor temperature is normally similar to the furnace temperature, the real reaction temperature with excited electrons could be much higher in the presence of plasma. Therefore, the reactor temperature was measured (within 10 s) by swiftly replacing the high-voltage (HV) electrode with a thermocouple in the center of the catalyst bed when the stable plasma-catalytic reaction is obtained. The measured reactor temperature was about 400 °C with the presence of plasma either empty or packed with alumina or the 15Co catalyst (Table S2†).

Recent work on plasma-assisted CO_2 and CH_4 reforming[25–28] shows mainly the production of CO, H_2 and oxygenates while only a small amount of higher hydrocarbons was reported. On the contrary, almost no oxygenates are detected in our system. Hence, we think the reaction process in our system is different from plasma-assisted dry reforming. We hypothesize that the formation of C_2^+ is mainly from plasma-driven activation and reaction of the produced methane. If the produced CH_4 is effectively converted *via* electron impact fragmentations (R1, R2), which is otherwise thermodynamically unfavorable even at 400 °C (R3, R4), the formation of higher hydrocarbons could be enhanced. To test our hypothesis, we have designed a series of catalyst-bed configurations for CO_2 hydrogenation to higher hydrocarbons under plasma (details of each configuration are given in the Table S1†). The obtained CO_2 conversion and product selectivity are presented in Fig. 2. The reactor temperature was also measured for different bed-configurations at different pre-marked positions for a better assessment of the temperature distribution under DBD plasma. As seen in Fig. S3 and Table S2,† when the furnace temperature is 250 °C at the plasma applied voltage of 13.6 kV, the temperature inside the reactor reaches about 400 °C for all configurations. The temperature distribution is relatively uniform within the entire bed.

Fig. 1 CO_2 conversion and product selectivity in the three different modes including catalyst alone, plasma alone and plasma-catalyst operated (a) without external heating and (b) at furnace temperature of 250 °C. Reaction conditions: 20 v% CO_2–60 v% H_2 in Ar balance, H_2/CO_2 = 3, flow rate = 20 mL min^{-1}, P = 1 atm, voltage = 13.6 kV, frequency = 23.5 kHz, plasma power = 4 W.

$$CH_3 - H + e^- \rightleftarrows CH_3^{\bullet} + H^{\bullet} + e^- \qquad (1)$$

$$H - CH_3 - H + 2e^- \rightleftarrows :CH_2 + 2H^{\bullet} + 2e^- \qquad (2)$$

$$2CH_4 \rightleftarrows C_2H_6 + H_2 \quad \Delta G\,(400°C) = 71 \text{ kJ mol}^{-1} \qquad (3)$$

$$3CH_4 \rightleftarrows C_3H_8 + H_2 \quad \Delta G\,(400°C) = 159 \text{ kJ mol}^{-1} \qquad (4)$$

In our DBD plasma reactor, gases flow vertically downward through the catalyst bed and the height of the discharge zone is fixed at 5 cm. The catalyst amount is first reduced from
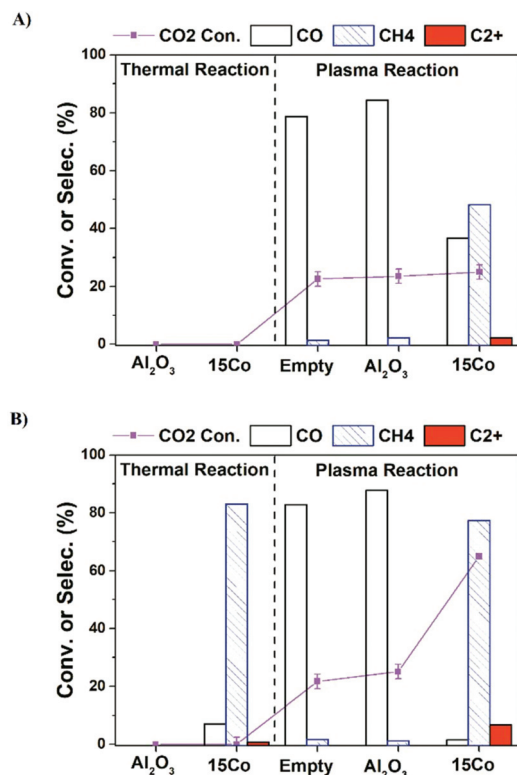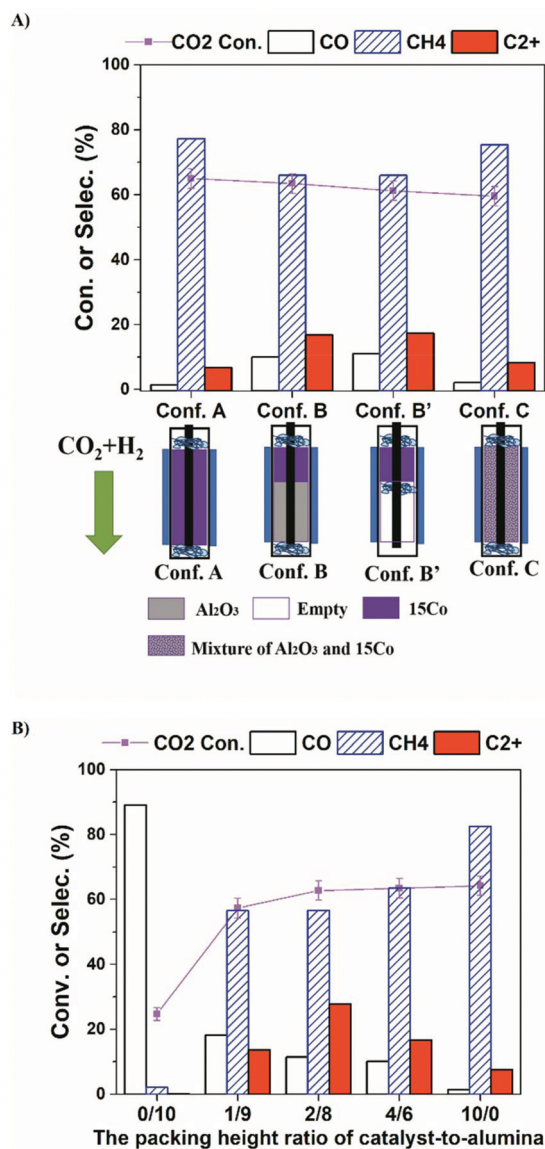
Fig. 2 Influence of catalyst-bed configuration (a) and catalyst-to-alumina ratio over **Conf. B** (b) on the CO_2 conversion and product distributions in the CO_2 hydrogenation over 15Co catalyst coupled with DBD plasma at the furnace temperature of 250 °C. Reaction conditions: 20 v% CO_2–60 v% H_2 in Ar balance, H_2/CO_2 = 3, flow rate = 20 mL min^{-1}, P = 1 atm, voltage = 13.6 kV, frequency = 23.5 kHz, plasma power = 4 W.

1.25 g (fully packed, termed as **Conf. A**) to 0.50 g, occupying only the top 2 cm of the discharge zone, while the rest is packed with γ-Al_2O_3 particles (termed as **Conf. B**, and noted as the ratio of 4/6 in the packing-height for catalyst-to-support). Compared to the discharge zone fully packed with the catalyst (**Conf. A**), **Conf. B** significantly enhances the selectivity towards C_2^+ hydrocarbons from 7% to 17%, while the CO_2 conversion stays the same (~62%). For a fair comparison, the same amounts of the catalyst and alumina support as those for the **Conf. B** are physically and homogeneously mixed, then packed fully within the discharge zone, which is termed as **Conf. C**.

Interestingly, methane again becomes the dominant product and the product distribution is very similar to that from the **Conf. A**, while the CO_2 conversion does not change significantly. The results clearly demonstrate that the configuration of the catalyst-bed significantly influences the reactions in plasma-enhanced CO_2 hydrogenation, resulting in the change in the product distributions. Compared to thermal catalysis at 400 °C, where only trace amount of C_2^+ hydrocarbons (1.4%) were formed (Table S4†), **Conf. B** seems to separate CH_4 formation and C–C coupling into two different packing portions with complementary properties, indicating the critical role of plasma for the formation of C_2^+ products. CO_2 is reduced to CH_4 over 15Co catalyst with plasma, whereas C–C coupling occurs within the alumina-packed plasma portion. Consequently, identification of the thermal-catalysis and plasma-catalysis contribution on the overall CO_2 hydrogenation to C_2^+ hydrocarbons over cobalt catalyst is crucial, which is under investigation in our laboratory.

The C_2^+ products are mainly C_2–C_5 paraffins along with some iso-paraffins and olefins, which are summarized in Table 1. Comparing **Conf. B** with **Conf. B′** (which has a similar bed configuration as **Conf. B** except no alumina packed in the second part of the discharge zone), there is no significant difference in both CO_2 conversion and products selectivity. No carbon deposition was observed on the reactor wall when using **Conf. B′**. In thermal catalytic reactions, acid sites on alumina usually work as active sites for isomerization or carbon deposition.[29,30] Here, the **Conf. B** and **Conf. B′** exhibit similar distributions in C_2^+ hydrocarbon product, iso/normal ratio (I/N), and olefin/paraffin ratio (O/P), indicating that the alumina-packing does not affect the methane conversion reactions, which occur in the gas phase and are driven by the plasma. Hence, we keep alumina packed for further study.

Fig. 2b illustrates the effect of the packing-height ratio between the 15Co catalyst and the alumina support in the discharge zone (**Conf. B**). Increasing the height of catalyst-packing increases the CO_2 conversion from 58% to 63%, whereas the overall C_2^+ selectivity increases first, reaching 27.8% at the packing-height ratio of 2/8, then decreases. When less catalyst is used (i.e., at the packing-height ratio of 1/9), less CO_2 is converted to methane. Consequently, the concentration of active CH_x species generated from methane activation by plasma is relatively low, which limits the carbon-chain growth in the second part of the bed. Hence, the overall C_2^+ selectivity at 1/9 ratio is low. The CO_2 molecules that have not been reduced to methane are further converted to CO in the alumina sector by plasma, leading to a higher CO selectivity. On the contrary, when more catalyst is packed (e.g., at the packing-height ratio of 4/6), the catalyst amount is sufficient to convert CO_2 at near equilibrium level as evidenced by the similar CO_2 conversion shown in Fig. 2b. However, the length of the alumina zone in plasma becomes relatively short, so does the residence time of plasma-activated CH_4 molecules, leading to less probability for carbon-chain propagation to higher hydrocarbons. Thereby, the selectivity of CH_4 increases while the C_2^+ selectivity decreases. As a result, the

Table 1 Distribution of hydrocarbon products in plasma–catalytic CO_2 hydrogenation with **Conf. B** and **Conf. B′**[a]

| Mode	Molar distribution[b] /%										Carbon balance/%	I/N[c]	O/P[d]
	$C_2^=$	C_2	$C_3^=$	C_3	i-C_4	$C_4^=$	n-C_4	i-C_5	$C_5^=$	n-C_5			
Conf. B	1.2	69.8	0.7	18.5	4.7	0.6	2.5	1.2	0.4	0.4	96	2.1	0.03
Conf. B′	2.5	65.8	1.1	19.4	5.1	1.0	2.9	1.4	0.4	0.4	97	2.0	0.05

[a] Furnace temperature = 250 °C; P = 1 atm; 20 v% CO_2–60 v% H_2 in Ar balance; total flow = 20 ml min^{-1}; voltage = 13.6 kV; frequency = 23.5 kHz; plasma power = 4 W. [b] Methane is not included here. [c] Iso-paraffins to normal paraffins molar ratio (C_4–C_5). [d] Olefins to paraffins molar ratio (C_2–C_5).

packing-height ratio of 2/8 gives the optimal C_2^+ production, for the investigated ratios.

It is worth mentioning that when 15Co catalyst is packed at the bottom 2 cm of the discharge zone, the performance is similar to those of **Conf. A** and **Conf. C** (Table S4†). Furthermore, when the total flow rate of the reactant gases increases, methane selectivity increases while the C_2^+ selectivity decreases as shown in Fig. S5.† The Lissajous figures in Fig. S6† display little change in the macro-scale plasma properties with different catalyst-bed configurations, suggesting that the dramatic change in C_2^+ production is mainly due to plasma-induced chemical reactions. These results suggest that both methane and CO are primary products, whereas C_2^+ hydrocarbons are secondary products forming from methane activation. It indicates that the generation of methane in the catalyst bed is essential for the production of higher hydrocarbons in the current plasma-catalyst system, likely through the reactions among the plasma-activated CH_x species.[7,31,32] Thus, we propose a possible C_2^+ formation mechanism in our system, which is described in Scheme 1. First, CO_2 is selectively reduced to CH_4 over 15Co catalyst under DBD plasma. Although CH_x species are simultaneously generated by plasma on the catalyst, they are quickly terminated by plasma-activated H species, leading to trace amount of C_2^+ hydrocarbons, as observed when the catalyst is fully packed (**Conf. A**). Within the alumina-packed portion, the plasma-activated CH_x species interact *via* gas-phase carbon-chain-growth reactions, generating more C_2^+ hydrocarbons. The proposed mechanism is supported by the fact that the distribution of C_2^+ products is very similar to that from the plasma methane conversion (Table S5†). However, spectroscopic analysis is needed to mechanistically understand reaction pathways, which is underway in our lab.

The production of C_2^+ hydrocarbons can be further enhanced *via* increasing the input plasma power. As shown in Fig. 3, higher CO_2 conversion is obtained over all cases by increasing plasma power to 10 W compared to the results in Fig. 1a (4 W). The selectivity to C_2^+ hydrocarbons is significantly improved. With **Conf. B** under a 10 W plasma at the furnace temperature of 25 °C (with no external heating), C_2^+ selectivity as high as 46.5% at CO_2 conversion of 74% (*i.e.*, C_2^+ hydrocarbons yield of 34.4%) is obtained. After 2 hours of reaction, we found the catalyst-bed temperature was about 400 °C. This is a result of inevitable heating effect of plasma and possibly the heat releasing from CO_2 hydrogenation to hydrocarbons.[18,20] Therefore, we have examined the thermal catalytic CO_2 hydrogenation at 400 °C without plasma (Table S3†). Although the CO_2 conversion is high (71%), the C_2^+ selectivity is only 1.4% while CH_4 selectivity is 92%. Such a difference strongly substantiates the key role of plasma and
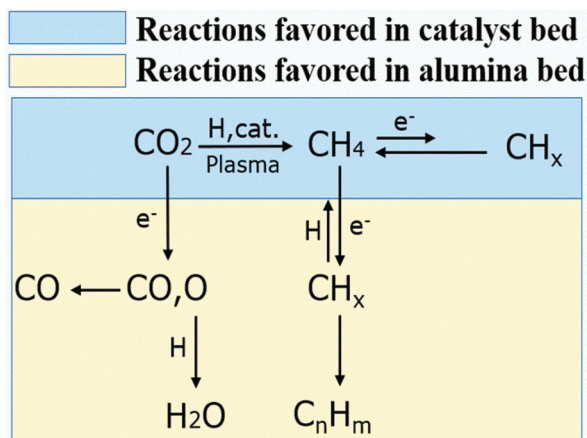
Scheme 1 The possible reaction pathways for higher hydrocarbons formation in the plasma promoted low-temperature CO_2 hydrogenation.
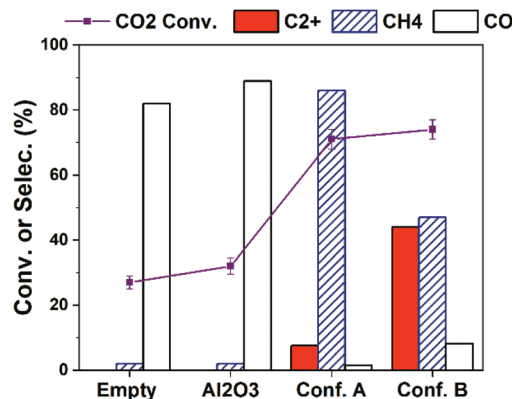

Fig. 3 Influence of catalyst-bed configuration on the CO_2 hydrogenation performance over 15Co catalyst under 10 W of DBD plasma at the furnace temperature of 25 °C. Reaction conditions: 20 v% CO_2–60 v% H_2 in Ar balance, H_2/CO_2 = 3, flow rate = 20 mL min^{-1}, P = 1 atm, voltage = 18.5 kV, frequency = 23.5 kHz.
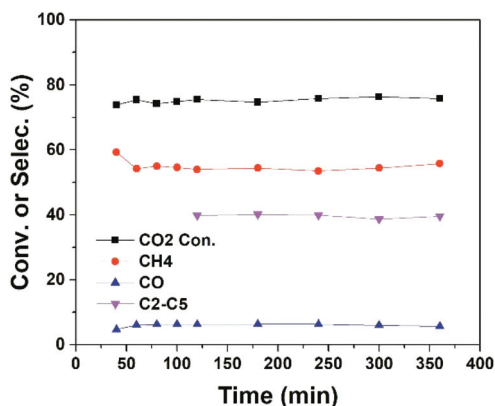
Fig. 4 CO_2 conversion and products selectivity as a function of time on stream (TOS) in CO_2 hydrogenation over 15Co catalyst under 7 W of DBD plasma at the furnace temperature of 250 °C. Reaction conditions: 17 v% CO_2–67 v% H_2 in Ar balance, H_2/CO_2 = 4, flow rate = 20 mL min^{-1}, P = 1 atm, voltage = 16.5 kV, frequency = 23.5 kHz.

catalyst-bed configuration in CO_2 hydrogenation to higher hydrocarbons.

In plasma methane conversion, carbon deposition is usually observed in the first few hours.[26,33] On the other hand, metal sintering is a common problem of cobalt catalyst in CO_2 hydrogenation.[14] Hence, we have examined the stability of the plasma catalytic process (**Conf. B**). As shown in Fig. 4, the reaction reaches steady state in a fairly short time and is stable for at least 6 hours of operation with plasma. No tendency of de-activation is observed, which can be attributed to the existence of plasma-induced active H or O radicals to remove deposited carbon and the ability of plasma to enhance metal dispersion and/or prevent metal agglomeration.[18,34,35]

In conclusion, our work clearly demonstrates the significant impact of the catalyst-bed configuration on plasma-catalytic CO_2 hydrogenation to higher hydrocarbons in one-step operated at low temperature and atmospheric pressure. With proper catalyst-bed configuration, high C_2^+ hydrocarbons selectivity of 46% at CO_2 conversion of over 70% is achieved. C_2^+ hydrocarbons are likely formed through the plasma-driven gas-phase methane conversion. Thus, the key in optimizing the catalyst-bed configuration is the balance between methane formation and plasma reactions for carbon-chain-growth from methane. It should also be pointed out that the catalyst used in this work is a conventional alumina-supported Co catalyst for Fischer–Tropsch synthesis. With further optimization of Co catalyst and/or development of more effective catalysts, the plasma-promoted catalytic CO_2 hydrogenation to higher hydro-carbons could be more promising. The present work may broaden the utilization of the plasma-catalyst synergy for effective CO_2 conversion to higher hydrocarbons.

Author contributions

Jiajie Wang: conceptualization, methodology, investigation, writing – original draft, visualization. Mohammad S. AlQahtani: methodology, writing – review & editing, visualization. Xiaoxing Wang: conceptualization, methodology, resources, writing – original draft, review & editing, visualization, project administration, supervision, funding acquisition. Sean D. Knech: resources, writing – review & editing, visualization. Sven G. Bilén: resources, writing – review & editing, visualization. Chunshan Song: conceptualization, resources, writing – review & editing, visualization, supervision, funding acquisition. Wei Chu: writing – review & editing.

Conflicts of interest

The authors claim no conflicts of interest.

Acknowledgements

References

1 R. Snoeckx and A. Bogaerts, *Chem. Soc. Rev.*, 2017, **46**, 5805–5863.

2 W. Wang, S. Wang, X. Ma and J. Gong, *Chem. Soc. Rev.*, 2011, **40**, 3703–3727.

3 A. Sternberg, C. M. Jens and A. Bardow, *Green Chem.*, 2017, **19**, 2244–2259.

4 H. Blanco and A. Faaij, *Renewable Sustainable Energy Rev.*, 2018, **81**, 1049–1086.

5 Q.-W. Song, Z.-H. Zhou and L.-N. He, *Green Chem.*, 2017, **19**, 3707–3728.

6 M. A. A. Aziz, A. A. Jalil, S. Triwahyono and A. Ahmad, *Green Chem.*, 2015, **17**, 2647–2663.

7 L. Wang, Y. Yi, H. Guo and X. Tu, *ACS Catal.*, 2017, **8**, 90–100.

8 W. Wang, X. Jiang, X. Wang and C. Song, *Ind. Eng. Chem. Res.*, 2018, **57**, 4535–4542.

9 R. Satthawong, N. Koizumi, C. Song and P. Prasassarakich, *Top. Catal.*, 2013, **57**, 588–594.

10 J. Wei, Q. Ge, R. Yao, Z. Wen, C. Fang, L. Guo, H. Xu and J. Sun, *Nat. Commun.*, 2017, **8**, 15174.

11 Z. Li, Y. Qu, J. Wang, H. Liu, M. Li, S. Miao and C. Li, *Joule*, 2019, **3**, 570–583.

12 G. Centi, E. A. Quadrelli and S. Perathoner, *Energy Environ. Sci.*, 2013, **6**, 1711.

13 Y. Gao, S. Liu, Z. Zhao, H. Tao and Z. Sun, *Acta Phys.-Chim. Sin.*, 2018, **34**, 858–872.

14 W. Li, X. Nie, X. Jiang, A. Zhang, F. Ding, M. Liu, Z. Liu, X. Guo and C. Song, *Appl. Catal., B*, 2018, **220**, 397–408.

15 A. Fridman, *Plasma Chemistry*, Cambridge University Press, 2008.

16 E. C. Neyts, K. K. Ostrikov, M. K. Sunkara and A. Bogaerts, *Chem. Rev.*, 2015, **115**, 13408–13446.

17 M. S. AlQahtani, S. D. Knecht, X. Wang, S. G. Bilén and C. Song, *ACS Catal.*, 2020, **10**, 5272–5277.

18 E. Jwa, S. B. Lee, H. W. Lee and Y. S. Mok, *Fuel Process. Technol.*, 2013, **108**, 89–93.

19 M. Nizio, A. Albarazi, S. Cavadias, J. Amouroux, M. E. Galvez and P. Da Costa, *Int. J. Hydrogen Energy*, 2016, **41**, 11584–11592.

20 M. Mikhail, P. Da Costa, J. Amouroux, S. Cavadias, M. Tatoulian, S. Ognier and M. E. Gálvez, *Catal. Sci. Technol.*, 2020, **10**, 4532–4543.

21 L. Lan, A. Wang and Y. Wang, *Catal. Commun.*, 2019, **130**, 105761.

22 B. Eliasson, U. Kogelschatz, B. Xue and L. Zhou, *Ind. Eng. Chem. Res.*, 1998, **37**, 3350–3357.

23 Y. Zeng and X. Tu, *IEEE Trans. Plasma Sci.*, 2016, **44**, 405–411.

24 A. H. Khoja, M. Tahir and N. A. S. Amin, *Energy Convers. Manage.*, 2019, **183**, 529–560.

25 L. Wang, Y. Yi, C. Wu, H. Guo and X. Tu, *Angew. Chem., Int. Ed.*, 2017, **56**, 13679–13683.

26 K. Krawczyk, M. Młotek, B. Ulejczyk and K. Schmidt-Szałowski, *Fuel*, 2014, **117**, 608–617.

27 J. Kim, D. B. Go and J. C. Hicks, *Phys. Chem. Chem. Phys.*, 2017, **19**, 13010–13021.

28 X. Tu and J. C. Whitehead, *Appl. Catal., B*, 2012, **125**, 439–448.

29 J. E. Samad, J. Blanchard, C. Sayag, C. Louis and J. R. Regalbuto, *J. Catal.*, 2016, **342**, 203–212.

30 J. Ni, L. Chen, J. Lin and S. Kawi, *Nano Energy*, 2012, **1**, 674–686.

31 A. Gómez-Ramírez, V. J. Rico, J. Cotrino, A. R. González-Elipe and R. M. Lambert, *ACS Catal.*, 2013, **4**, 402–408.

32 L. Wang, S. Y. Liu, C. Xu and X. Tu, *Green Chem.*, 2016, **18**, 5658–5666.

33 A. H. Khoja, M. Tahir and N. A. S. Amin, *Energy Convers. Manage.*, 2017, **144**, 262–274.

34 W. Chu, L. N. Wang, P. A. Chernavskii and A. Y. Khodakov, *Angew. Chem., Int. Ed.*, 2008, **47**, 5052–5055.

35 M. S. AlQahtani, X. Wang, J. L. Gray, S. D. Knecht, S. G. Bilén and C. Song, *J. Catal.*, 2020, **391**, 260–272.